Journal of Solid State Chemistry **143,** 277–284 (1999)
Article ID jssc.1998.8109, available online at http://www.idealibrary.com on IDEAL®

Structure and Properties of 1256 and 1267 Type $Hg_{1-x}Re_xBa_2Ca_{n-1}Cu_nO_{2n+2+4x+\delta}$ Single Crystals

H. Schwer, R. Molinski, E. M. Kopnin, G. I. Meijer, and J. Karpinski

Laboratorium für Festkörperphysik, ETH Hönggerberg, 8093 Zürich, Switzerland

Received July 30, 1998; in revised form November 15, 1998; accepted November 14, 1998

Single crystals of $Hg_{0.75}Re_{0.22}Ba_2Ca_5Cu_6O_{15}$ and of $Hg_{1-x}Re_xBa_2Ca_6Cu_7O_{16+4x+\delta}$ have been grown with a gas-phase high pressure technique at 10 kbar. They crystallize in space group $P4/mmm$ with lattice parameters $a = 3.8542(3)$ Å, $c = 25.162(3)$ Å (HgRe-1256) and $a = 3.8514(5)$ Å, $c = 28.388(7)$ Å (HgRe-1267). They represent the $n = 6$, 7 members of the layered cuprate superconductors of the type $HgBa_2Ca_{n-1}Cu_nO_{2n+2+\delta}$. X-ray single crystal structure analysis showed that Re doping decreases the size of the rock-salt block. Rhenium substitutes mercury up to 25% and forms short bonds of 1.86 Å to oxygen atoms. They coordinate Re octahedrally and are shifted off their ideal positions to (0.34, 0.34, 0). The crystals contain stacking faults which are included in the refinements. In the HgRe-1267 crystal they are so numerous that they influence the refinement severely. A simulation of the Fourier maps proved that observable maxima in the difference electron density map are in fact due to stacking faults. The transition temperature onset of HgRe-1256 is 100 K and that of HgRe-1267 is assumed to be 84 K.

1. INTRODUCTION

The Hg–Ba–Ca–Cu–O system is the most promising system to obtain superconductors with high transition temperatures. The highest $T_c = 133$ K was reached with the compound $HgBa_2Ca_2Cu_3O_{8+\delta}$ (1), which could be increased to 164 K under high pressure (2). Until now, we obtained single crystals of the $n = 1$–5 members of the homologous series $HgBa_2Ca_{n-1}Cu_nO_{2n+2+\delta}$ (Hg-12($n-1$)n) with a gas-phase high pressure technique from various fluxes (3). In literature, there are to our knowledge only two reports on single crystals with $n > 5$ CuO_2 layer materials: Akimoto *et al.* (4) grew mercury free (C,Cu)-1256 crystals, and Bertinotti *et al.* (5) reported about Hg-1267 crystals.

Recent studies showed that Re doping may increase flux pinning leading to a high B_{irr} (6). In order to carry out corresponding experiments on single crystals we grew crystals which incorporated rhenium substituting up to 25% of mercury atoms. Besides known phases of HgRe-1223, -1234, and -1245 we obtained several crystals with c parameters of about 25.2 Å and one crystal with $c = 28.388$ Å. It turned out that they belonged to the six and seven CuO_2 layer structure type 1256 and 1267. Another reason for Re doping is the structural stabilization of mercury based phases by introduction of high valence ions such as rhenium (7, 8).

First structural investigations on (Re, Hg) based superconductors have been carried out by Chmaissem *et al.* (9, 10) with neutron diffraction on ceramic samples of HgRe-1212, -1223, and -1234. The main effect which has been observed upon Re doping was the occurrence of four additional oxygen atoms in the basal layer connected to rhenium. Since we have already structural data of $n = 1$–5 $HgBa_2Ca_{n-1}Cu_nO_{2n+2+\delta}$ single crystals (11), these new crystals give the opportunity to complete our crystal chemical knowledge about the transition from one layer Hg-1201 to infinite layer $CaCuO_2$ within this homologous series. In this paper, we present the results of X-ray single crystal structure analyses and magnetic measurements of these new HgRe-1256 and HgRe-1267 crystals.

2. EXPERIMENTAL

Crystals were grown with a gas-phase high-pressure technique using a 3 kbar Nova Swiss gas compressor and a pressure intensifier with an internal three zone Kanthal furnace (3). The Hg-12($n-1$)n compounds melt peritectically, but at ambient pressure they decompose before melting and the volatile components evaporate. The evaporation of Hg is suppressed by using Ar gas which has a high density at high pressures. As a flux we used a mixture of $BaCuO_2$, CuO, and Ag_2O. This was mixed with reacted Hg-1201, Ca_2CuO_3, CuO, and ReO_2 and heated to a maximum temperature $T = 1040$–1025°C at Ar pressures $p_{Ar} = 10.0$–10.2 kbar. The samples were cooled down by 20°C at a rate of 2–20°C/hour, followed by a rapid cooling to room temperature.

The superconducting transition temperature T_c was determined from the dc magnetization, $M(T)$, measured with a BTI SQUID magnetometer. The data were taken in the

0022-4596/99 $30.00

zero-field cooled mode for 1256 and both field cooled and zero-field cooled mode for the 1267 crystal with magnetic field applied parallel to the *c*-axis. Three 1256 crystals have been measured and the transition onset, defined by the deviation of the magnetization from the zero baseline, ranges between 92 and 100 K. As shown in Fig. 1, the mid-transition (defined as 50% of the full transition) temperature is only 3 K below the onset, with a small transition width ΔT_c (10–90%) of about 6 K. The sharpness of the transition is a good indication for the high quality of the 1256 crystals. The 1267 crystal has the onset of the transition at 100 K and two steps at 90 K and at 84 K. It can be suspected that this step at 84 K corresponds to the onset of T_c of the 1267 phase; in this case the onset of 100 K is attributed to the big number of stacking faults of 1256 material which was observed in the structure analysis of this 1267 crystal. The relatively high FC magnetization is indicative for a large Meissner fraction in the crystal.

Additional magnetization measurements were performed on a HgRe-1256 single crystal, with $T_c = 92$ K (12). The irreversibility line was determined by measuring hysteresis loops $M(H)$ and field cooled/zero-field cooled $M(T)$ data. From the cross-over field $B_{cr} = 430$ Oe, the anisotropy was estimated to about $\gamma \approx 70$. This value is consistent with the general trend of the Hg-12$(n-1)n$ family. Other results of magnetization measurements will be published separately.

The crystals were examined with a Buerger precession X-ray single crystal camera, using Mo$K\alpha$ radiation ($\lambda =$ 0.7107 Å). As expected, they had tetragonal symmetry and lattice parameters $a = 3.85$ Å and $c = 25.2$ Å and 28.4 Å, respectively. The crystals are black, rectangular plates, the main face is (001), and the edges usually run parallel to the *a*-axes. Three 1256 crystals which showed sharp diffraction spots and no traces of twinning or macroscopic intergrowth were selected for diffractometer measurements. We found only one 1267 crystal which was not intergrown. Unfortunately, the reflections have been broader as usual; however, since this was the only 1267 crystal we obtained, we decided to measure it on the single crystal diffractometer, despite the poor quality.

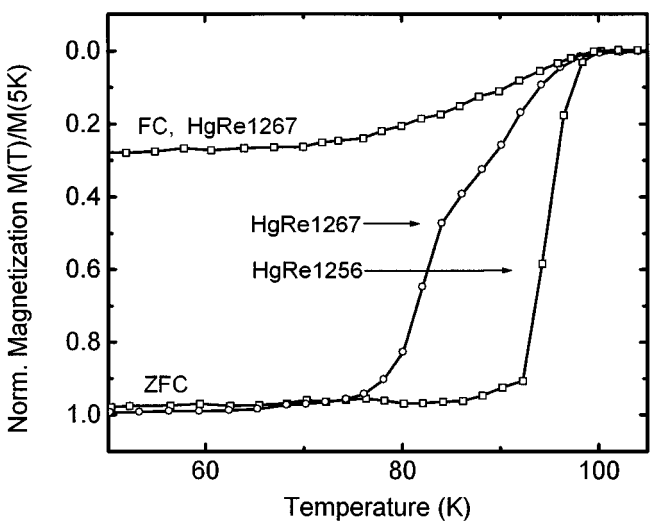

FIG. 1. DC magnetization measurements of a HgRe-1256 (ZFC) and a HgRe-1267 (FC + ZFC) crystal.

3. STRUCTURE ANALYSIS OF HgRe-1256

Three crystals have been measured on an X-ray four-circle Siemens P4 single crystal diffractometer. Structure analyses of the crystals have been quite similar, therefore data collection conditions and refinement parameters for only one 1256 crystal are listed in Table 1.

A total of 6698 reflection profiles of the whole Ewald sphere have been recorded with the ω-scan. After every 97

TABLE 1
Data Collection and Refinement Parameters for HgRe-1256

Formula	$Hg_{0.75}Re_{0.22}Ba_2Ca_5Cu_6O_{15}$
Formula weight	1287.73 g/mol
Crystal size	$0.25 \times 0.18 \times 0.02$ mm^3
Color	black
Diffractometer	Siemens P4
Monochromator	Graphite
Radiation	Mo$K\alpha$ ($\lambda = 0.71073$ Å)
Temperature	293K
a	3.8542(3) Å
c	25.162(3) Å
V	379.79(7) Å^3
Z	1
Space group	*P*4/*mmm* (No. 123)
Density ρ_x	5.721 g/cm^3
μ (Mo$K\alpha$)	24.77 mm^{-1}
Scan mode	ω-scan
2Θ range	2–70°
h, *k*, *l*	$-6 \le h \le 6;\ -6 \le k \le 6;\ -40 \le l \le 40$
No. of measured reflections	6698
No. of unique reflections	608
Transmission min.	0.0548
Transmission max.	0.6355
R_{int} (F^2)	0.066
No. of refined parameters	48
Refinement method	full matrix least squares on $\|F^2\|$
F_{000}	582.5
$R1^a$ (all data), $R1^a$ ($F_o > 4\sigma$)	0.038, 0.032
w$R2^b$ (all data)	0.083
Goodnes of fit, S^c (all data)	1.266
$\Delta\rho_{max}$ at *x*, *y*, *z*	3.9 electrons/Å^3 at 0, 0, 0.14
Weighting factor^d *a*, *b*	0.0429, 1.64
Extinction factor^e *y*	0.012(1)

$^a R1 = \sum ||F_o| - |F_c|| / \sum |F_o|$.
^{b} w$R2 = [\sum (w(F_o^2 - F_c^2)^2 / \sum (w(F_o^2)^2]^{1/2}$.
$^c S = [\sum (w(F_o^2 - F_c^2)^2 / (N_{refl} - N_{par})]^{1/2}$.
$^d w = 1/[\sigma^2 F_o^2 + (a(1/3F_o^2 + 2/3F_c^2)^2 + b(1/3F_o^2 + 2/3F_c^2)]$.
$^e F_c = F_c k[1 + 0.001 y F_c^2 \lambda^3 / \sin(2\Theta)]^{-1/4}$. k, overall scale factor.

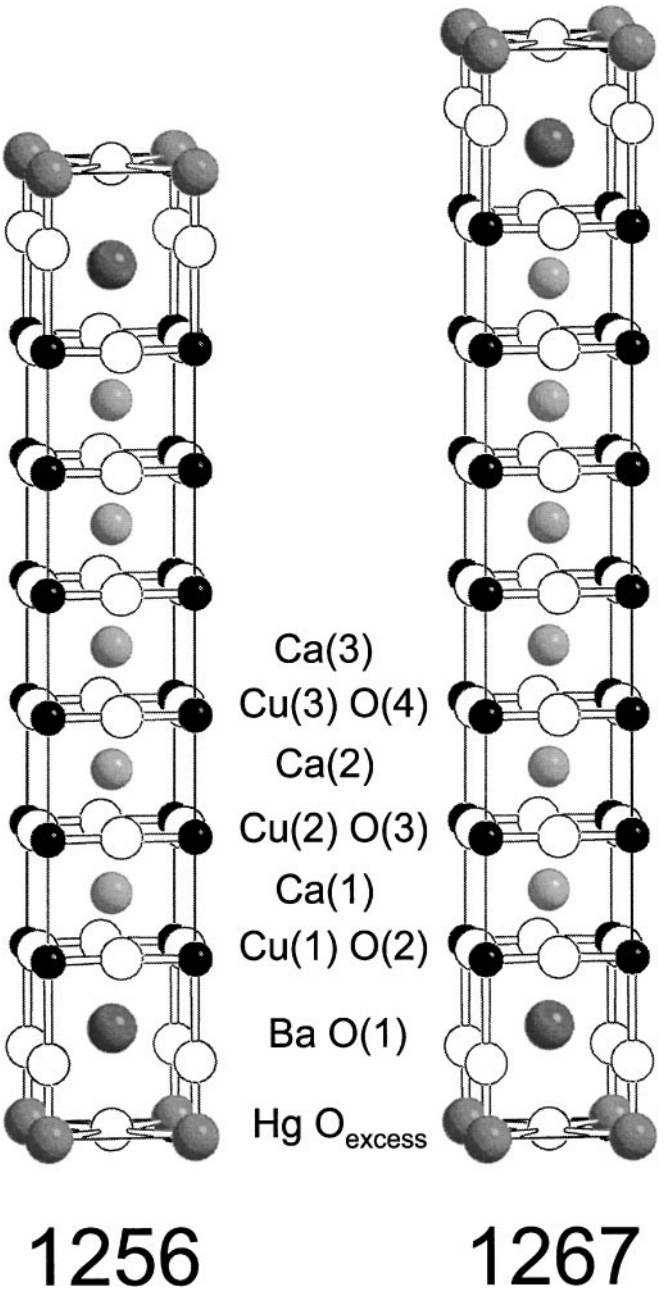

FIG. 2. Crystal structures of 1256 and 1267 types.

collected intensities three check reflections have been measured in order to notice a possible intensity decrease. The variation of check reflections was below $\pm 1.5\%$. Data have been corrected for Lorentz and polarization effects and reflection profiles have been fitted to an averaged learnt profile. All of the following data handling procedures and calculations are performed with the SHELXTL program (13). Absorption corrections have been applied to the data with the linear absorption coefficient by calculating the beampath through the crystal for each reflection. The crystal is defined by faces and their distances to a common point. After absorption correction intensity data have been averaged to 608 symmetry independent ("unique") data according to the Laue class 4/*mmm*.

The initial structural parameters for the refinement were calculated from the idealized 1256 structure type (Fig. 2). After several refinement cycles we observed distinct maxima in the difference electron density map (ΔF) at (0, 0, 0.127) with 11.9 electrons/Å^3, at ($\frac{1}{2}$, $\frac{1}{2}$, 0.018) with 9.1 electrons/Å^3, t ($\frac{1}{2}$, $\frac{1}{2}$, 0.231) with 6.5 electrons/Å^3, and at (0.352, 0.352, 0) with 5.8 electrons/Å^3 which are shown in Fig. 3b. They are already visible in the corresponding electron density map in Fig. 3a.

The last peak at (0.352, 0.352, 0) is attributed to oxygen atoms connected with rhenium. The first three strong peaks are due to the effects of stacking faults and they occur frequently in this class of layered cuprates with more than three CuO_2 layers (11, 14, 15). They are attributed to virtual atoms Hg′, Ba1′, and Ba2′ which are generated by a ghost image of the crystal structure shifted by the distance between two adjacent CuO_2 layers in *c*-direction. With inclusion of all these features in the refinement, the final agreement factors converged to $R = 0.032$ (F-data) and w$R2 = 0.083$ (F^2-data). The resulting composition for this crystal is $Hg_{0.75}Re_{0.22}Ba_2Ca_5Cu_6O_{15}$ and refined structural parameters are given in Table 2. Without inclusion of the Hg′, Ba1′, and Ba2′ atoms the refinement converged with $R = 0.041$ and w$R2 = 0.106$. The structural parameters remained the same within their error limits, except for the Ba content which was refined to 0.931(7) and the Ca(1) position ($z/c = 0.24487(8)$). This shift is due to the electron density of Ba2′ which overlaps with that of Ca(1) and therefore, gives a different average z/c parameter of "Ca(1)". Bondlengths of this "Ca(1)" to oxygen are less uniform (Ca(1)–O(2) = 2.431(3) Å, Ca(1)–O(3) = 2.544(3) Å) than those of the "true" Ca(1) site at $z/c = 0.24514(8)$.

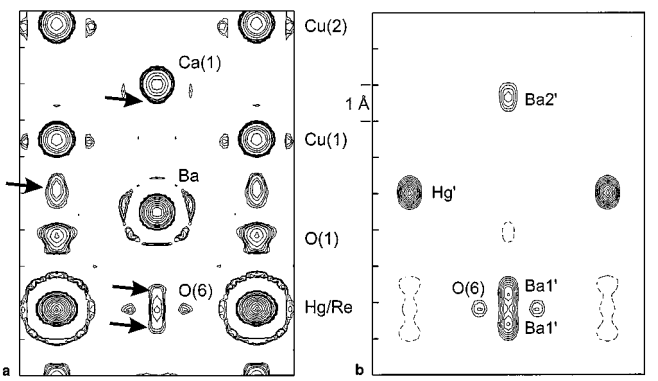

FIG. 3. Electron (a) and difference electron (b) density maps of the (110) section of the 1256 crystal structure. Arrows point to the electron densities due to stacking faults in (a).

TABLE 2
Structure Data for $Hg_{0.75}Re_{0.22}Ba_2Ca_5Cu_6O_{15}$, space group *P4/mmm*, $a = 3.8542(3)$ Å, $c = 25.162(3)$ Å

Atom	Site	Occ	*x/a*	*y/b*	*z/c*	U_{11} [Å^2]	U_{22} [Å^2]	U_{33} [Å^2]
Hg[a]	1a	0.69(2)	0	0	0	0.0183(2)	0.0183(2)	0.0051(2)
Re[a,c]	1a	0.22(2)	0	0	0	0.0183(2)	0.0183(2)	0.0051(2)
Ba[b,d]	2h	0.878(3)	1/2	1/2	0.10488(2)	0.0079(2)	0.0079(2)	0.0074(3)
Ca(1)	2h	1	1/2	1/2	0.24514(8)	0.0057(5)	0.0057(5)	0.0048(6)
Ca(2)	2h	1	1/2	1/2	0.37312(4)	0.0056(4)	0.0056(4)	0.0053(6)
Ca(3)	2h	1	1/2	1/2	1/2	0.0066(6)	0.0066(6)	0.0020(7)
Cu(1)	2g	1	0	0	0.18410(4)	0.0042(3)	0.0042(3)	0.0088(5)
Cu(2)	2g	1	0	0	0.31022(4)	0.0029(3)	0.0029(3)	0.0069(4)
Cu(3)	2g	1	0	0	0.43684(4)	0.0031(3)	0.0031(3)	0.0065(4)
O(1)	2g	1	0	0	0.0781(3)	0.014(2)	0.014(2)	0.013(3)
O(2)	4i	1	1/2	0	0.1859(2)	0.002(2)	0.010(2)	0.013(2)
O(3)	4i	1	1/2	0	0.3110(2)	0.004(2)	0.007(2)	0.011(2)
O(4)	4i	1	1/2	0	0.4369(2)	0.004(2)	0.006(2)	0.011(2)
O(5)[c]	1c	0.12(4)	1/2	1/2	0	0.011(5)	0.011(5)	0.011(5)
O(6)[c,e]	4j	0.22(2)	0.344(4)	0.344(4)	0	0.011(5)	0.011(5)	0.011(5)
Hg′[a,f]	2g	0.061(3)	0	0	0.1260(5)	0.0183(2)	0.0183(2)	0.0050(2)
Ba1′[b,d,f]	2h	0.061(3)	1/2	1/2	0.0208(7)	0.0079(2)	0.0079(2)	0.0074(3)
Ba2′[b,d,f]	2h	0.061(3)	1/2	1/2	0.2308(9)	0.0079(2)	0.0079(2)	0.0074(3)

[a,b,c]Constrained to the same U_{ij}.
[d]Constrained to 100% occupancy.
[e,f]Constrained to the same occupancy.

4. DISCUSSION

Selected bondlengths of $Hg_{0.75}Re_{0.22}Ba_2Ca_5Cu_6O_{15}$ are presented in Table 3. Lattice parameters *a* are in the same range as those of undoped crystals with more than three CuO_2 layers (11), whereas $c/(n+2)$ is clearly shorter. Comparison with powder data of Capponi *et al.* (16) and Scott *et al.* (17) shows that *c* is about 0.1 Å shorter than in undoped material. CuO_2 interlayer spacings, Ca–O, and Ba–O(2) bondlengths are the same as in $Hg12(n-1)n$ with $n > 3$; therefore, the perovskite block is not affected by doping or by inserting an additional CuO_2 layer. These distances are also in agreement with those reported by Akimoto *et al.* (4) for Cu-1256. The main changes occur in the rock-salt block: partial substitution of Hg by the smaller Re decreases this part of the structure and the *c* lattice parameter. This is expressed by significantly shorter Hg–Ba (3.794 Å) and Ba–O(1) (2.807 Å) distances than in undoped crystals (3.85 and 2.85 Å, respectively). The blocking layer thickness (Ba–Ba) decreases by 0.2 Å from 5.48 Å in Hg-1245 to 5.28 Å in 1256 due to Re-doping.

TABLE 3
Selected Bondlengths in $Hg_{0.75}Re_{0.22}Ba_2Ca_5Cu_6O_{15}$

Atoms	Distance	Atoms	Distance
Hg/Re–Ba	3.794(1) Å	Ca(1)–O(2)	2.436(3) Å
		Ca(1)–O(3)	2.541(3) Å
Hg/Re–O(1)	1.965(8) Å	Ca(2)–O(3)	2.482(3) Å
Hg–O(5)	2.725(0) Å	Ca(2)–O(4)	2.509(3) Å
Re–O(6)	1.86(2) Å	Ca(3)O(4)	2.496(3) Å
Ba–O(1)	2.807(1) Å	Cu(1)–O(1)	2.667(8) Å
Ba–O(2)	2.806(4) Å	Cu(1)–O(2)	1.928(0) Å
Ba–O(5)	2.639(1) Å	Cu(2)–O(3)	1.927(0) Å
Ba–O(6)	2.776(7) Å	Cu(3)–O(4)	1.927(0) Å

Rhenium ($Z = 75$) replaces partially mercury ($Z = 80$), but due to their almost equal scattering powers for X rays, it is not possible to distinguish them in the refinement. The Re content is determined indirectly: The difference electron density map of the basal plane in Fig. 4 shows two different maxima which are attributed to different oxygen atoms. Rhenium forms short bonds < 2 Å, if it is coordinated octahedrally. The distance of O(6) at (0.344, 0.344, 0) to the Hg/Re atom is 1.86 Å—a bondlength which is close to usually observed Re–O bonds, and which is far too short for a Hg–O bond (≈ 2.75 Å) in this class of superconductors. Therefore, the amount of O(6) is four times as high as that of rhenium and the occupation factors of Re and O(6) have been constrained to the same value during the refinement, resulting in a ReO_4 content of 0.22 in the basal plane. In contrast to Pb doping (14, 15), the Fourier maps do not show shifts of the dopant off the Hg site. Another difference to other $12(n-1)n$ structure refinements is the almost full occupation (97%) of the Hg/Re site.

Figure 4 shows a second electron density maximum at ($\frac{1}{2}$, $\frac{1}{2}$, 0) consisting of a superposition O(5) and Ba1′ electron

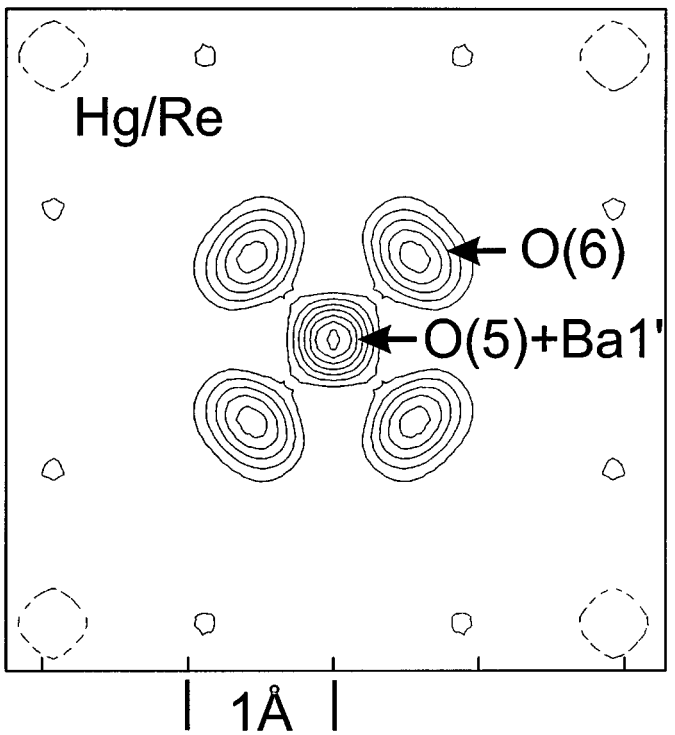

FIG. 4. Difference electron density map of the basal plane of HgRe-1256, containing Hg/Re and O(5,6) atoms.

densities. Ba1′ is due to the presence of stacking faults and will be discussed in the next section; O(5) is excess oxygen connected to mercury. A model of the basal Hg/Re–O plane is given in Fig. 5. One unit cell cannot carry more than one oxygen atom which is either connencted to Hg or to Re. It is impossible that two adjacent rhenium atoms exist with an octahedral oxygen coordination, because in this case two O(6) atoms with a distance of about 1.73 Å from each other would be necessary in one unit cell. This is far too short for stability reasons and, therefore, a maximum Re substitution of 25% is possible in HgRe-12$(n-1)n$.

5. STACKING FAULTS

The problem of stacking faults in $HgBa_2Ca_{n-1}Cu_nO_{2n+2+\delta}$ and the way of solving this problem have already been discussed in Refs. (11, 14, 15). The most common defects in layered materials are stacking faults. During crystal growth the stacking sequence of layers may be easily disturbed because the difference of free energies for continuing a given stacking sequence with the same or a slightly different stacking sequence is very small. The more similar are the main and the defect phase, the higher is the probability for the generation of stacking faults; therefore, the number of stacking faults is increasing from about 2% in 1223 to 5% in 1245 (11) and to finally about 6% in 1256 and 10% in

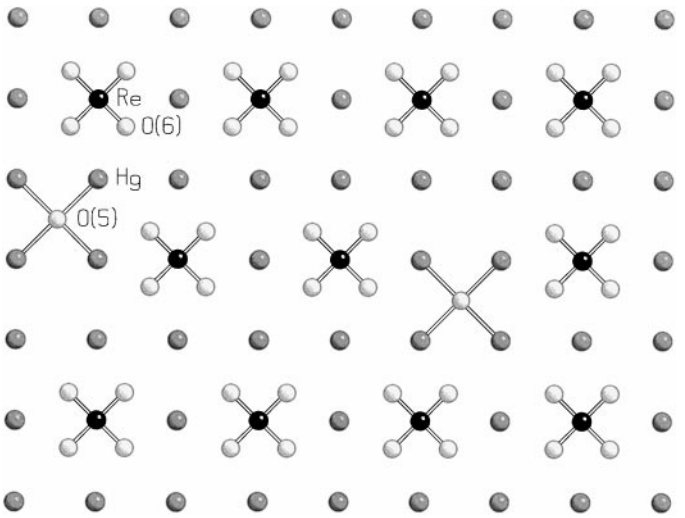

FIG. 5. Model of the basal plane in HgRe-12$(n-1)n$ crystal structures.

1267. The number of stacking faults is expressed by the average ratio of $12n(n+1)$ or $12(n-2)(n-1)$ unit cells (single stacking faults) to $12(n-1)n$ unit cells (main phase) stacked in c direction. These amounts are only typical average values refined in good single crystals showing uniform peak shapes without streaks or intergrowth peaks in precession photographs. Of course, the number of stacking faults varies from crystal to crystal but the trend goes clearly as mentioned above. In general, four out of five crystals are not suitable for structure analysis because of intergrowth or irregular peak shapes due to large amounts of stacking faults. HRTEM photographs of such crystals or polycrystalline material showed a much higher content of defects than almost perfect crystals with undistorted stackings of several hundred ångströms.

The ΔF map in Fig. 3 shows the maxima exactly at those positions, which are expected in the presence of stacking faults (e.g., 11). The largest peak is between Hg and apical oxygen O(1) at $(0, 0, 1/(n+2))$, two further peaks are close to Ca and to $(\frac{1}{2}, \frac{1}{2}, 0)$ at $(\frac{1}{2}, \frac{1}{2}, z(\mathrm{Ba}) - 1/(n+2))$, and at $(\frac{1}{2}, \frac{1}{2}, z(\mathrm{Ba}) + 1/(n+2))$. These peaks form a ghost image of the heavy atom structure of 1256 which is shifted by the vector $(0, 0, \pm 1/(n+2))$, pointing from one CuO_2 layer to the next one. The corresponding distances are Hg–Hg′ = 3.170 Å, Ba–Ba1′ = 3.162 Å, and Ba–Ba2′ = 3.168 Å, nearly the same as the Cu–Cu distances in c-direction (3.18 Å).

In order to give a further proof for the validity of this model where the peaks are due to stacking faults, we simulated the corresponding Fourier maps. We calculated the structure factors F_{id} of an ideal structure model, and F_{sf} of models containing 5 and 10% stacking faults with the program PRECPLOT (18). For example, the 5% model consisted of 38 unit cells $12(n-1)n$, one cell $12n(n+1)$, and one unit cell $12(n-2)(n-1)$ stacked in c direction. The

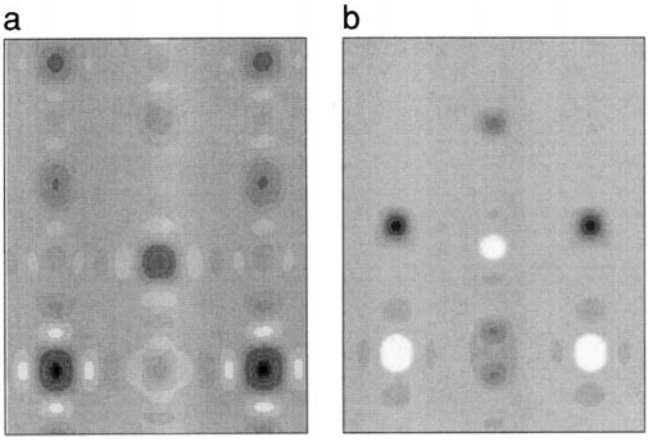

FIG. 6. Simulation of the electron density maps in Fig. 3 with FOURDEM. (a) Electron density map of the (110) section the ideal Hg12$(n-1)n$ model; (b) the ΔF map with the maxima caused by stacking faults.

Fourier summation was performed with the program FOURDEM (19) and is presented in Fig. 6. The left image shows the Fourier summation of the ideal model with $|F_{id}|$ and ϕ_{id} and corresponds to the electron density map in Fig. 3(a). The right image is calculated with $|F_{sf}| - |F_{id}|$ and ϕ_{id} and corresponds to the difference electron density map. It represents the real situation, when a ΔF map is calculated from diffraction data of a real crystal with stacking faults $|F_{sf}|$ and of the refined structure model $|F_{id}|$ and ϕ_{id}. As in Fig. 3b the maxima in the difference Fourier map appear at those positions, which are shifted away from the atom positions in real space by the vector pointing from one layer to the adjacent one. It was even possible to quantify at least empirically the number of stacking faults with this simulation: the maxima increase linearly with the number of stacking faults in the model, and the ratio of the Hg′/Hg electron density is about 0.06 and 0.12 for the 5 and 10% stacking fault models, respectively (20). Moreover, this simulation also yields the negative electron densities at the positions of the Hg and Ba atom, which are also observed in Fig. 3b. They appear as white dots in the simulation in Fig. 6b and are negative if the average gray background is set to zero level.

One big problem is the exact determination of the true excess oxygen content, because the electron density of O_{excess} at $(\frac{1}{2}, \frac{1}{2}, 0)$ is hidden under the overlapping peaks of Ba1′. This was done by constraining the occupancies of Hg′, Ba1′, and Ba2′ to the same value and by simultaneously constraining the sum of the site occupations of Ba, Ba1′, and Ba2′ to 100%. The remaining electron density at the $(\frac{1}{2}, \frac{1}{2}, 0)$ site was then attributed to O_{excess}, whose occupancy was refined to 0.12. The content of Hg′, Ba1′, and Ba2′ atoms is proportional to the number of stacking faults and is refined to 6.1(3)%. It should be emphasized that these stacking faults may be present in every member of the homologous Hg-12$(n-1)n$ series for $n \geq 2$, even if crystals seem to be absolutely single crystalline; of course, in ceramic material these stacking faults are also existing. A good example is given by Chmaissem *et al.* (10) who found in a Rietveld refinement of ceramic material also a defect close to $(\frac{1}{2}, \frac{1}{2}, 0)$; they attributed it to displaced oxygen atoms but it appears exactly at the position of Ba1′ indicating the presence of stacking faults.

6. STRUCTURE ANALYSIS OF HgRe-1267

As mentioned above, we found only one crystal of HgRe-1267 which was not twinned or intergrown. Precession photographs showed that the reflections are broadened and elongated in c^*. This is a hint for the presence of a rather big number of stacking faults, as well as the magnetization (Fig. 1) showing two steps. Nevertheless, we decided to measure this crystal on the diffractometer, simply because we only found this one of 1267 type. The lattice parameters are $a = 3.8514(5)$ Å and $c = 28.388(7)$ Å. A total of 7406 reflections have been collected from the whole Ewald sphere. After absorption correction the intensities have been averaged to 673 unique F^2 data with an internal $R_i = 0.2$. The thermal parameters have been refined to unreasonable anisotropic values, giving very high U_{33} up to 0.029 Å^2 and very small U_{11} and U_{22} close to 0.001 Å^2. Therefore, Table 4 lists only U_{eq} together with positional parameters. Final w$R2$ is 0.36 for F^2 data and $R = 0.14$ for F data; the goodness of fit is $S = 1.15$.

As expected, the amounts of Hg′, Ba1′, and Ba2′ are quite large with 9.6(9)%, supporting the model of an increase of the number of stacking faults with increasing number of CuO_2 layers in the main phase. Therefore, the electron density of the excess oxygen at $(\frac{1}{2}, \frac{1}{2}, 0)$ is completely hidden under the Ba1′ electron density. It is even impossible to refine oxygen connected with rhenium, because the Ba1′ electron density is distributed over a large area in the basal plane. Figure 7 shows the ΔF map of the basal plane in the 1267 crystal; the O(6) peaks at (0.34, 0.34, 0) are visible but the atom position and occupation cannot be refined. For this reason it is also impossible to determine the Re amount, because it is usually defined about the occupation factor of O(6). Another problem concerns the O(1) position: in the presence of a large number of stacking faults, even the ghost image Cu′ of the Cu(1) atom appears, unfortunately close to the O(1) position. For this reason the O(1) site cannot be resolved clearly and the refined fractional coordinate of O(1) might be doubtful. The resulting bondlengths are in the range of those of HgRe-1256, except those to the apical O(1) atom.

In the literature there exists only one study about 1267: Bertinotti *et al.* (5) found a crystal with a lattice parameter $c = 28.520(5)$ Å and a $T_c = 132$ K. According to Scott *et al.* (17) T_c for 1267 should not be higher than 90 K like in our

TABLE 4
Structure Data for (HgRe)$Ba_2Ca_6Cu_7O_{16+\delta}$, Space Group *P4/mmm*, $a = 3.8514(5)$ Å, $c = 28.388(7)$ Å

Atom	Site	Occ	x/a	y/b	z/c	U_{eq} [Å^2]
Hg[a]	1a	0.73(2)	0	0	0	0.0109(8)
Ba[b,d]	2h	0.808(9)	$\frac{1}{2}$	$\frac{1}{2}$	0.0948(1)	0.0116(7)
Ca(1)	2h	1	$\frac{1}{2}$	$\frac{1}{2}$	0.2191(3)	0.004(1)
Ca(2)	2h	1	$\frac{1}{2}$	$\frac{1}{2}$	0.3321(2)	0.003(1)
Ca(3)	2h	1	$\frac{1}{2}$	$\frac{1}{2}$	0.4438(2)	0.003(1)
Cu(1)	2g	1	0	0	0.1643(2)	0.0027(8)
Cu(2)	2g	1	0	0	0.2760(2)	0.0014(7)
Cu(3)	2g	1	0	0	0.3878(2)	0.0023(8)
Cu(4)	2g	1	0	0	$\frac{1}{2}$	0.003(1)
O(1)	2g	1	0	0	0.061(2)	0.01(1)
O(2)	4i	1	$\frac{1}{2}$	0	0.1654(8)	0.011(4)
O(3)	4i	1	$\frac{1}{2}$	0	0.2765(7)	0.005(3)
O(4)	4i	1	$\frac{1}{2}$	0	0.3884(7)	0.007(3)
O(5)	4i	1	$\frac{1}{2}$	0	$\frac{1}{2}$	0.006(4)
O(6)[c]	4j		0.34	0.34	0	
Hg′[a,e]	2g	0.096(9)	0	0	0.111(1)	0.109(8)
Ba1′[b,d,e]	2h	0.096(9)	$\frac{1}{2}$	$\frac{1}{2}$	0.010(2)	0.116(7)
Ba2′[b,d,e]	2h	0.096(9)	$\frac{1}{2}$	$\frac{1}{2}$	0.208(3)	0.116(7)
Cu′[e]	2g	0.096(9)	0	0	0.054(3)	0.109(8)

[a,b]Constrained to the same U_{ij}.
[c]Not refined.
[d]Constrained to 100% occupancy.
[e]Constrained to the same occupancy.

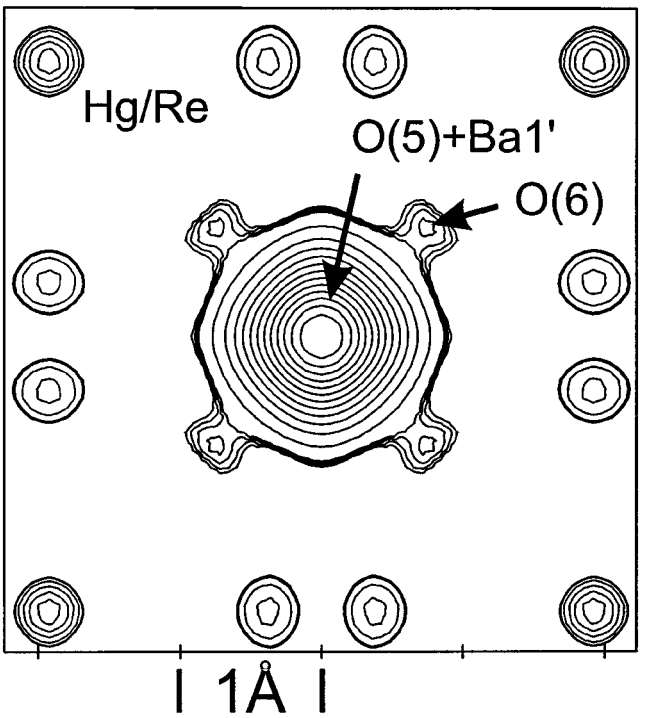

FIG. 7. Difference electron density map of the basal plane in HgRe-1267.

HgRe-1267 crystal. As Bertinotti *et al.* have not yet performed a structure analysis of their crystal it seems plausible that their crystal consists of an ordered intergrowth phase of 1212 and 1223. The *c* lattice parameters in these intergrowth phases are the sums of the parameters of the individual $12(n-1)n$ phases and would be in this case $c_{1212} + c_{1223} \approx 28.52$ Å. This "Hg-2435" phase was already observed in small grains by HRTEM with a *c*-parameter of 28.6 Å (21). Recently, we found a whole crystal of "HgRe-2457," consisting of an ordered alternating stacking of 1223 and 1234 units with $c = 34.377$ Å (22).

7. CONCLUSIONS

With a gas-phase high pressure technique we grew single crystals of $Hg_{0.75}Re_{0.22}Ba_2Ca_5Cu_6O_{15}$ and of $Hg_{1-x}Re_xBa_2Ca_6Cu_7O_{16+4x+\delta}$ at 10 kbar Ar pressure and at a maximum temperatures of 1040 °C. The maximum transition temperature is 100 K for HgRe-1256; the onset of the transition of the HgRe-1267 crystal is also 100 K, but T_c of the 1267 phase is assumed to be 84 K.

X-ray single crystal structure analysis showed that rhenium substitutes mercury up to 25%. Re is coordinated octahedrally by oxygen and forms short bonds of 1.86 Å. O(6) is displaced off its ideal positions to (0.34, 0.34, 0).

Substitution of Hg by the smaller Re atoms decreases the size and the bondlengths in the rock-salt block of the structure. The perovskite unit is not affected by this process and has comparable dimensions and bondlengths like other Hg-12$(n-1)n$ structures.

With increasing *n* the crystals contain increasing amounts of stacking faults. They are included in the structure analysis and are refined to 6.1(3)% in HgRe-1256 and to 9.6(9)% in HgRe-1267.

The stacking faults introduce additional electron densities close to the position of the O_{excess} atom at $(\frac{1}{2}, \frac{1}{2}, 0)$. In the case of HgRe-1256 this effect could be corrected, but in HgRe-1267 the stacking faults are so numerous that a refinement of the oxygen atoms in the basal plane was not possible.

In order to prove the validity of the stacking fault model we simulated the Fourier maps. Calculation of theoretical (difference) electron density maps proved that observable maxima in the ΔF maps are in fact caused by stacking faults and that their intensities are proportional to their amount.

ACKNOWLEDGMENTS

This work was supported by the Swiss National Foundation. We are grateful to P. Wägli who analyzed the crystals by EDX.

REFERENCES

1. A. Schilling, M. Cantoni, J. D. Gao, and H. R. Ott, *Nature* **363,** 56 (1993).
2. L. Gao, Y. Y. Xue, F. Chen, Q. Xiong, R. L. Meng, D. Ramirez, C. W. Chu, J. H. Eggert, and H. K. Mao, *Phys. Rev. B* **50,** 4260 (1994).
3. J. Karpinski, H. Schwer, R. Molinski, G. I. Meijer, K. Conder, E. Kopnin, J. Löhle, C. Rossel, D. Zech, J. Hofer, A. Wisniewski, and R. Puzniak, *in* "Studies of High Temperature Superconductors" (A. Narlikar, Ed.), Vol. 24, p. 165. Nova Science. Commack, NY, 1997.
4. J. Akimoto, K. Tokiwa, A. Iyo, H. Ihara, H. Hayakawa, Y. Gotoh, and Y. Oosawa, *Physica C* **279,** 181 (1997).
5. A. Bertinotti, D. Colson, J.-F. Marucco, V. Viallet, G. Le Bras, L. Fruchter, C. Marcenat, A. Carrington, and J. Hammann, *in* "Studies of High Temperature Superconductors" (A. Narlikar, Ed.), Vol. 24, p. 56. Nova Science, Commack, NY, 1997.
6. J. Shimoyama, S. Hahakura, R. Kobayashi, K. Kitazawa, K. Yamafuji, and K. Kishio, *Physica C* **235–240,** 2795 (1994).
7. J. Shimoyama, K. Kishio, S. Hahakura, K. Kitazawa, K. Yamaura, Z. Hiroi, and M. Takano, "Advances in Superconductivity VII," (K. Yamafuji and T. Morishita, Eds.), p. 287. 1994. Springer Verlag, Tokyo.
8. R. L. Meng, B. R. Hickey, Y. Y. Sun, Y. Cao, C. Kinalidis, J. Meen, Y. Y. Xue, and C. W. Chu, *Physica C* **260,** 1 (1996).
9. O. Chmaissem, J. D. Jorgensen, K. Yamaura, Z. Hiroi, M. Takano, J. Shimoyama, and K. Kishio, *Phys. Rev B* **53,** 14647 (1996).
10. O. Chmaissem, P. Guptasarma, U. Welp, D. G. Hinks, and J. D. Jorgensen, *Physica C* **292,** 305 (1997).
11. H. Schwer and J. Karpinski, *in* "Studies of High Temperature Superconductors" (A. Narlikar, Ed.), Vol. 24, p. 49. Nova Science, Commack, NY, 1997.
12. M. Angst, diploma work ETH Zürich, 1998; to be published.
13. G. M. Sheldrick, SHELXTL-5, Siemens Analytical X-Ray Instruments, 1994.
14. H. Schwer, J. Karpinski, K. Conder, L. Lesne, C. Rossel, A. Morawski, T. Lada, and A. Paszewin, *Physica C* **243,** 10 (1995).
15. H. Schwer, J. Karpinski, L. Lesne, C. Rossel, A. Morawski, T. Lada, and A. Paszewin, *Physica C* **254,** 7 (1995).
16. J. J. Capponi, E. M. Kopnin, S. M. Loureiro, E. V. Antipov, E. Gautier, C. Chaillout, B. Souletie, M. Brunner, J. L. Tholence, and M. Marezio, *Physica C* **256,** 1 (1996).
17. B. A. Scott, E. Y. Suard, C. C. Tsuei, D. B. Mitzi, T. R. McGuire, B.-H. Chen, and D. Walker, *Physica C* **230,** 239 (1994).
18. H. Schwer, PRECPLOT, program for simulation of precession photographs, University of Freiburg, Germany, (1990).
19. T. R. Welberry and K. Owen, *J. Appl. Cryst.* **25,** 443 (1992).
20. H. Schwer *et al.*, in preparation.
21. Y. S. Yao, W. Liu, Y. J. Su, Y. F. Xiong, W. J. Ma, G. H. Cao, G. T. Zou, and Z. X. Zhao, *Physica C* **282–287,** 897 (1997).
22. H. Schwer, R. Molinski, E. M. Kopnin, M. Angst, and J. Karpinski, *Physica C* **311,** 49 (1999).